Marine Geology 255 (2008) 156–164

Contents lists available at ScienceDirect

Marine Geology

journal homepage: www.elsevier.com/locate/margeo

Low-Energy Rip Currents Associated With Small Bathymetric Variations

Jamie H. MacMahan [a,*], Ed B. Thornton [a], Ad J.H.M. Reniers [b,c], Tim P. Stanton [a], Graham Symonds [d]

[a] Naval Postgraduate School, Oceanography Department, Monterey, CA, 93943, USA
[b] Civil Engineering and Geosciences, Delft University of Technology, Delft, The Netherlands
[c] Rosenstiel School of Marine and Atmospheric Science, University of Miami, Miami, USA
[d] CSIRO Marine and Atmospheric Research, Private Bag No. 5, Wembley Way, 6913, Australia

ARTICLE INFO

Article history:
Received 5 February 2008
Received in revised form 4 August 2008
Accepted 15 August 2008

Keywords:
rip currents
non-uniformity
morphodynamics
nearshore
surf zone
circulation

ABSTRACT

We show for the first time that low-energy waves can induce a rip current system over subtle alongshore bathymetric variations. Comprehensive field measurements across a rip current that morphologically migrated (~ 12 m/day) through a coherent cross- and alongshore array of co-located pressure and velocity sensors were obtained. The rip current is associated with a small bathymetric surfzone non-uniformity (1 in 300 alongshore variation). The circulation was kinematically non-uniform for ~5% of the time over the course of the 20 day experiment and was present at low tides associated with increases in rip current activity. The presence of the rip current and mild-sloped rip channel induce statistically significant alongshore variations in $H_{rms,}$ wave direction, directional spreading, infragravity waves, and very low frequency motions. Changes in the directional spreading are correlated with the presence of very low frequency motions influenced by the presence of the rip current.

Published by Elsevier B.V.

1. Introduction

Rip currents are strong, jet-like, seaward-directed flows that originate within the surf zone owing to alongshore gradients in wave-induced radiation stresses and pressure (Bowen, 1969; Dalrymple, 1978; Haller et al., 2002). Long and Okzan-Haller (2005) showed that refraction of waves travelling across offshore submarine canyons can create variations in wave height alongshore that induce rip currents in the absence of local surfzone bathymetric non-uniformity. In contrast, most field observations of rip currents to date have been coupled to variations in the surfzone alongshore bathymetry, which induce alongshore differences in the wave forcing (Shepard et al., 1941; Shepard and Inman, 1950; Sonu, 1972; Aagaard et al., 1997; Brander and Short, 2001, MacMahan et al., 2005), but the development of the bathymetric non-uniformity remains unclear. Furthermore, the degree to which surfzone bathymetric non-uniformities induce a hydrodynamic response, in particular a rip current, is unknown. We show for the first time that low-energy waves can induce a rip current system with subtle alongshore bathymetric variations.

Within the last decade, more quantitative field and laboratory observations of rip currents have become available (Aagaard et al., 1997; Brander, 1999; Brander and Short, 2000, 2001; Haller and Dalrymple, 2001; Haas and Svendsen, 2002; Haller et al., 2002; Callaghan et al., 2004; MacMahan et al., 2005, MacMahan et al., submitted for publication). Most of these rip current field experiments have explored rip currents on beaches that support persistent, energetic rip currents. However, there have been few comprehensive field observations of rip current hydrodynamics owing to the difficulty of deploying instruments in a rip channel, and in part because of the tendency for the rip channels to migrate alongshore. During the Nearshore Canyon Experiment (NCEX) in fall 2003 at Torrey Pines, California, a morphologically controlled rip current fortuitously migrated slowly through an extensive cross- and alongshore array of co-located electromagnetic current meters and pressure sensors over ~10 days. The kinematics of this low-energy rip current system and the corresponding subtle rip morphology are described.

2. Field site

2.1. In situ observations

Field observations were obtained during NCEX (October 29 to November 18, 2003; yeardays 302–322). The beach is characterized as near planar with a surfzone slope of 1:70 between $50 \geq x \geq -75$ and an offshore slope of 1:50 between $-75 \geq x \geq -200$, where the cross-shore distance is positive onshore (see Fig. 1). Two primary arrays were deployed: 1) an alongshore array of 6 pressure and bi-directional digital electromagnetic current meters, dems, spanning approximately 500 m, and 2) a cross-shore array of 6 pressure and dems ranging from the shoreline to a depth of 3.5 m. Incorporated into the cross-shore array were 8 paroscientific pressure sensors (paros), 6 of which were co-located with the 6 cross-shore dems. Pressure and dem

* Corresponding author.
E-mail address: jhmacmah@nps.edu (J.H. MacMahan).

0025-3227/$ – see front matter. Published by Elsevier B.V.
doi:10.1016/j.margeo.2008.08.006

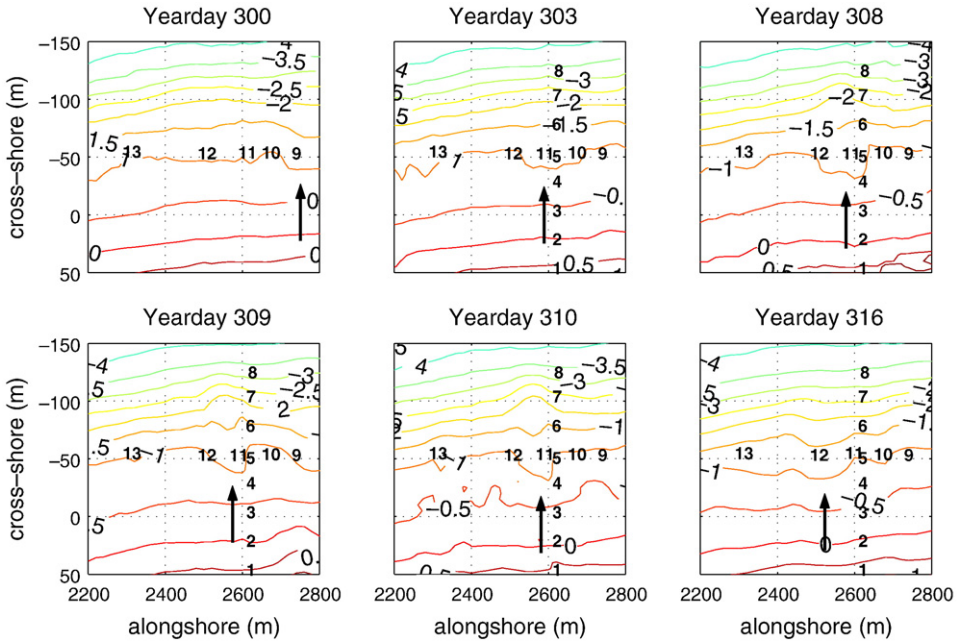

Fig. 1. Bathymetry referenced to mean sea level (MSL) for yeardays 300, 303, 308, 309, 310, and 316. Bold numbers represent co-located pressure and velocity instruments. Arrows represent rip channel locations, which are referred to in the text.

sensors were sampled continuously and synchronously at 15 Hz, while the paros were sampled at 1 Hz. The dems were approximately 35 cm off the sea bed, except PUV8, which was 1 m off the sea bed.

Directional wave spectra were measured with an upward-looking, broad-band, acoustic Doppler current profiler located in approximately 6 m water depth ($x=-246$ m) in line with the cross-shore array. During the measurement period, the significant wave height (H_{mo}) ranged 50–125 cm, the mean wave period ranged 3.5–12 s, and the mean wave direction ranged −12° to +12° (Fig. 2). Only a few moderate storm events occurred during the experiment, near the onset and at the end of the measurement period (yeardays 304, 320, and 322). Hourly mean alongshore currents averaged over the alongshore array ranged between −75 cm/s to +25 cm/s. Rip current activity occurred for yeardays 303, and 306–315, during which time H_{mo} was approximately

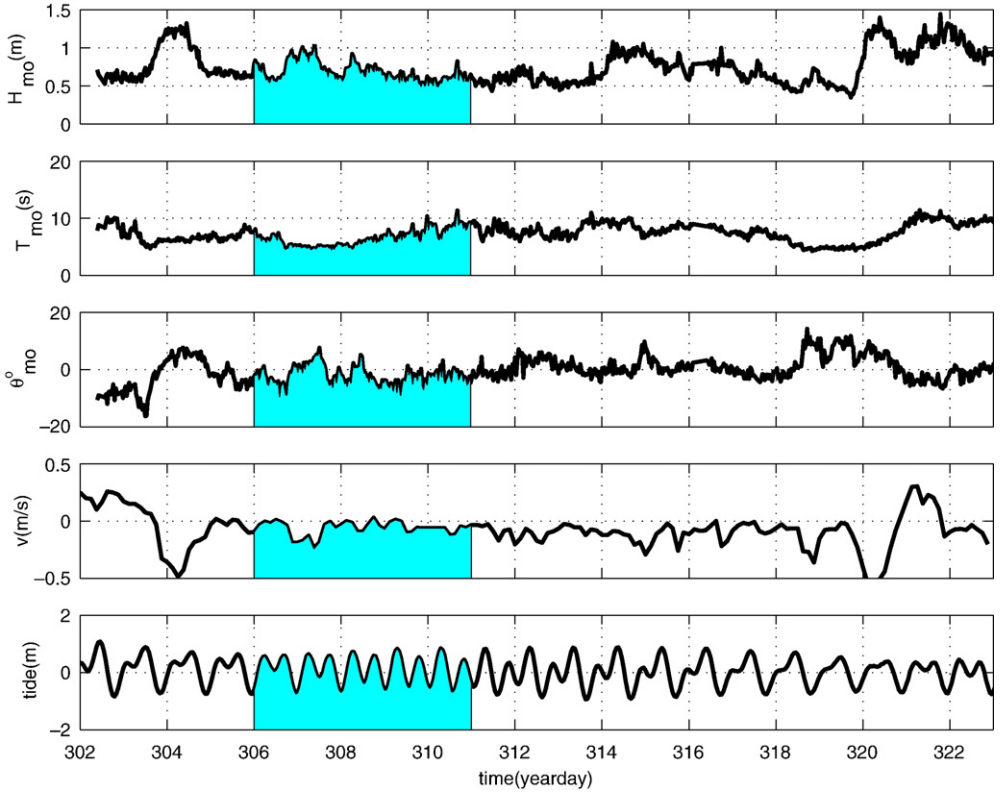

Fig. 2. Wave climate measured by directional ADCP in 6 m water depth, approximately 250 m offshore: significant wave height, H_{mo} (top), mean wave period (second), peak wave direction (third), alongshore-averaged mean alongshore velocity (fourth), and tidal elevation (bottom). Shaded region represents period of rip current activity.

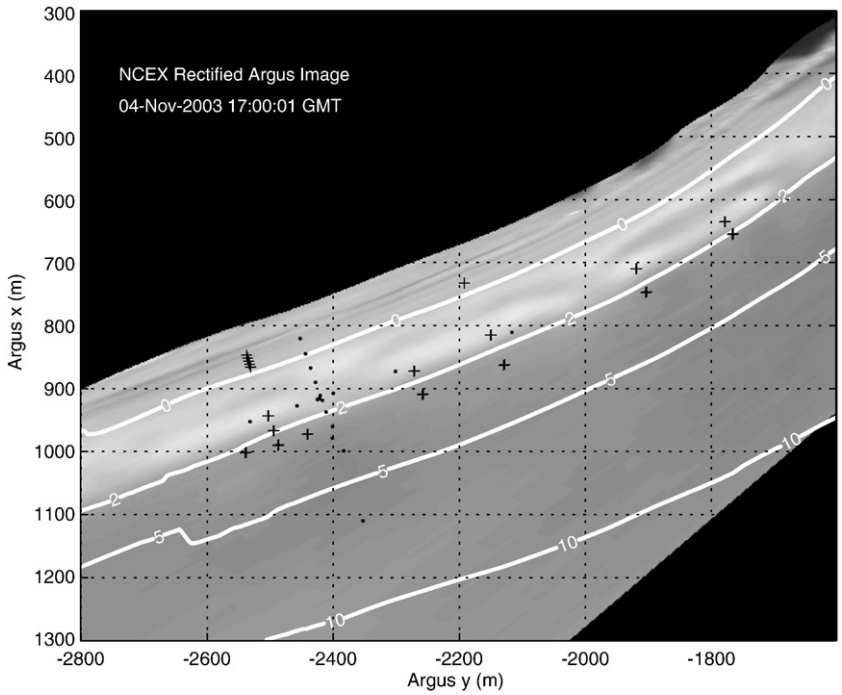

Fig. 3. Time-averaged Argus video image at low tide (yearday 308) depicting the nearshore breaking wave patterns and the underlying rip current morphology. Bathymetry is in meters. Dots represent the NPS arrays. Crosses represent the Scripps and WHOI arrays.

50 cm, the wave direction was predominantly shore-normal, and the alongshore current was ~0 cm/s (Fig. 2).

2.2. Bathymetric observations

Bathymetric surveys were obtained at high tide using a hydrographic surveying system composed of a GPS and sonar mounted onboard a personal water craft. The upper beachface was surveyed at low tide with a GPS mounted on a cart. These surveys were performed 6 times between yeardays 300–316 with the last survey performed 7 days before the end of the experiment (Fig. 1). Rip channels are identified as perturbations on the otherwise straight bathymetry contours, either as a depression inside the surfzone cut by the rip current (contours indented shoreward) and as accretionary feature outside the surfzone formed by sediment deposition from the rip current (contours bulged seaward).

The rip current morphology has ~140±30 m channel width based on the bathymetry plots in Fig. 1. The rip spacing is ~300–400 m based the quasi-periodic dark regions located inline with the outer bar in the rectified time-averaged video image of wave breaking intensities for yearday 308 (Fig. 3). Depth-limited wave breaking occurs on the bar outlining shallow regions, while the deeper sections of the rip channel have minimal wave breaking and appear darker. Shepard and Inman (1950) had previously observed rip currents at Torrey Pines with an alongshore spacing of 500 m. The depth variation across the rip channel is ~0.25 m in 75 m alongshore (Fig. 1). It is noted that the rip channel morphology is very broad with the bathymetric variation smaller than the camber (0.5–1%) of an athletic playing field (www.drainage.org).

The bathymetry for yearday 300 suggests that a rip channel has developed at the 1 m (x=40 m) contour around y=2800 (Fig. 1). At yearday 303, the rip channel increased in width and migrated south to y=2600 in the vicinity of the cross-shore array. The rip channel slowly migrated south during yeardays 308–310. In addition, the bathymetric contours seaward of the rip channel bend seaward suggesting localized accretion. The rip channel system continued to migrate south, but by yearday 316 it becomes less pronounced. No additional surveys exist past yearday 316.

3. Morphologically-controlled migrating rip currents

3.1. Coherent alongshore array

The migration of the rip current is examined using hourly mean cross-shore velocities computed for the alongshore array. The magnitude and the direction of the cross-shore flow varies at each instrument (Fig. 4). Though a mean alongshore current (0.15 cm/s) is present for yearday 303 two rip currents are identified in the cross-shore flow at PUV10 and PUV 13 (~360 m apart). At the same time a slight onshore flow occurs at PUV9 at low tide and returns to an offshore flow at higher tides. The onshore flow of PUV9 is associated with cellular circulation of a rip current at PUV10 (80 m to the south) (Haller et al., 2002). The rip current cells of PUV10 and PUV13 are believed to be independent, as smaller intervening offshore flows occur for PUVs 5, 11, and 12. During the later part of yearday 303, the alongshore current reverses direction to a downcoast orientation and quickly increases in magnitude to 50 cm/s, which abruptly ceases the two rip currents at PUV10 and PUV13 (Fig. 2). The alongshore currents are believed to have caused the rip circulation to cease, allowing subtle rip current morphology to persist and migrate downcoast.

Following the small storm, onshore flow ceases at PUV9 and migrates to PUV10 for a few hours surrounding low tides on yeardays 304–307 (Fig. 5), after which the flows return to an offshore orientation, representative of undertow. The onshore flow at PUV10 is associated with cellular circulation of a rip current (offshore flows) at PUV5 and PUV11 (40 and 60 m to the south). The rip current is centered near PUV11, approximately 25 m to the south of PUV5, where strong offshore flows were measured for yeardays 306–310. Slightly smaller offshore flows occur at PUV5, the location of the cross-shore array, than PUV11 for yeardays 305–309, representative of a rip current. Midday on yearday 309, the flow reversed onshore at low tide at PUV5 for yeardays 309–312. After yearday 310, the flow reversed to an onshore flow at low tides at PUV 11 for the next four days, similar to PUVs 5 and 10. There was stronger offshore flow at PUV12 (100 m south of PUV11) indicative of a rip current for yeardays 314–318. The offshore flow during rip current activity at PUV12 is reduced in overall

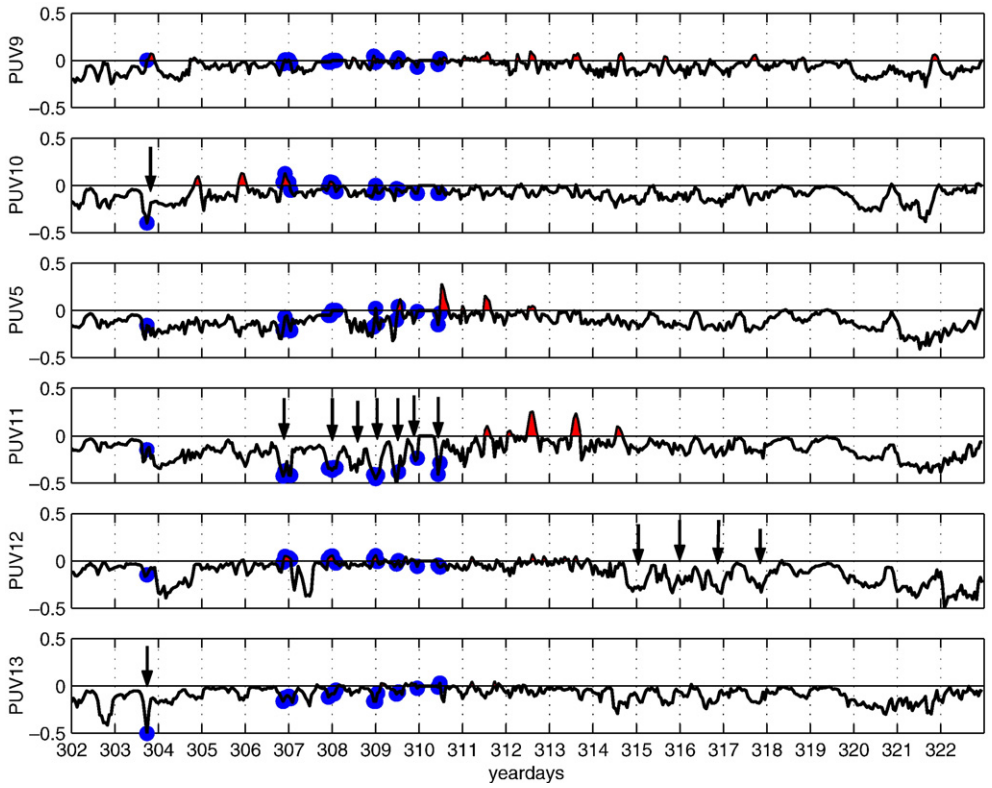

Fig. 4. Hourly mean cross-shore velocities (m/s) for the alongshore array. Shaded regions emphasize onshore flow. Circles represent times of kinematic non-uniformity. Arrows highlight rip currents described in Section 3.1.

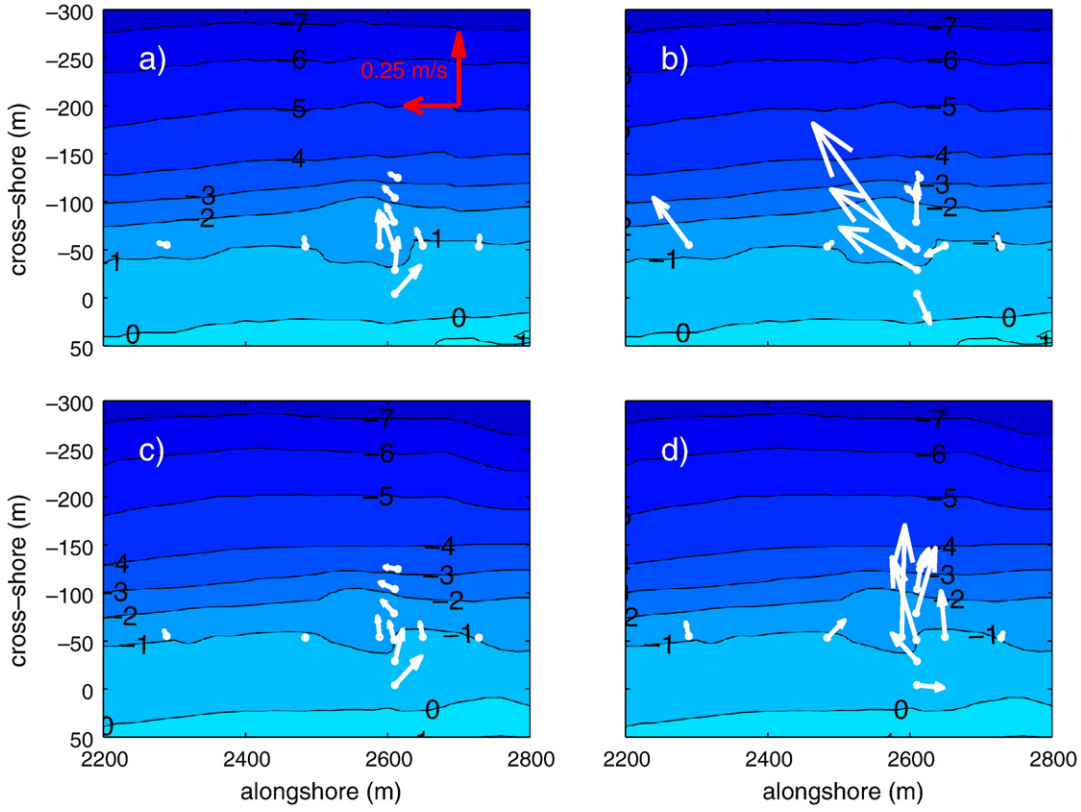

Fig. 5. Hourly mean velocity vectors for high (left) and low (right) tide during the period when rip currents were present in the alongshore array for yeardays 306 (a, b) and 309 (c,d). Red vectors are 0.25 m/s scale. Bathymetric contours are plotted in the background.

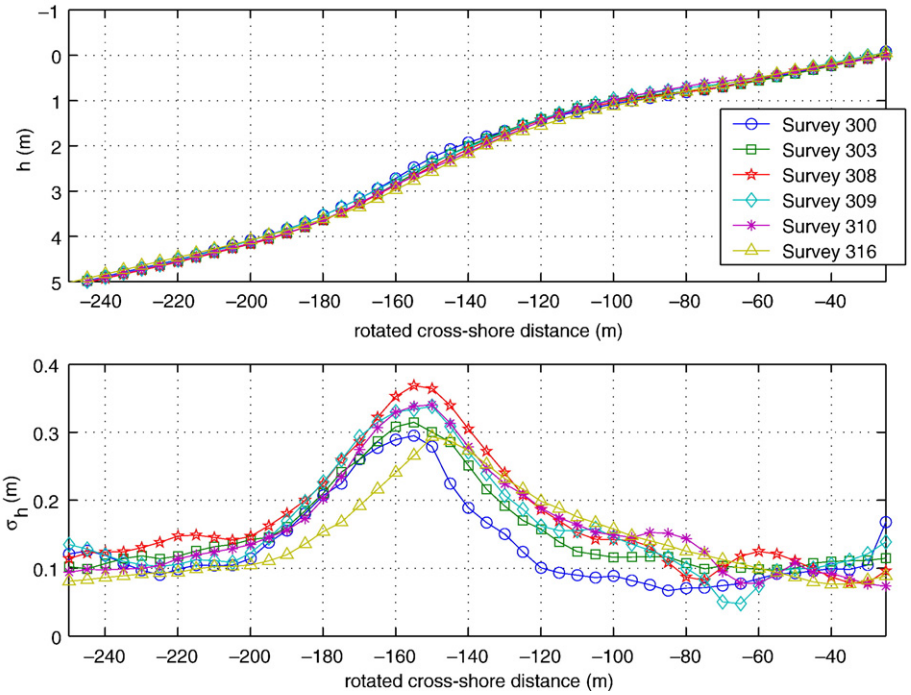

Fig. 6. The mean alongshore bottom profile, $\overline{h(x')}$ (top), and alongshore depth variation, $\sigma_h(x')$ (bottom), for yeardays 300, 303, 308, 309, 310, and 316.

magnitude comparative to the rip activity at PUV11. In summary, a rip current is active modifying the flow field for PUVs 5, 10, 11 for yeardays 306–311.

The time difference between the first onshore flow peak at PUV10 and PUV5 is approximately 4.5 days over a distance of 50 m, which corresponds to an 11 m/day migration rate. The time difference between the first onshore peak at PUV5 and PUV11 is approximately 2 days over a distance of 25 m, which corresponds to a 12.5 m/day migration rate. The time difference between the first offshore peak at PUV11 and PUV12 is approximately 8 days over a distance of 100 m, which corresponds to a 12.5 m/day migration rate. This suggests that the rip current migrated down-coast supporting the temporally sparser bathymetric observations.

3.2. Low-energy rip current circulation patterns

Hourly mean velocity vectors are used to examine the nearshore circulation during low and high tides for two rip current cases associated with non-uniform bathymetry when the waves were normally incident (yeardays 306 and 309) (Fig. 5). The nearshore circulation on yearday 306 at high tide shows the strongest offshore flows occurring closest to shore and within the rip channel (Fig. 5a). At high tide, the offshore flow is qualitatively larger within the rip channel compared to the offshore flows measured by the adjacent instruments in the alongshore array. During low tide, both the rip current and adjacent off-shore flows increase, but the currents within the rip channel are comparatively larger (Fig. 5b). The localized offshore delta identified as a seaward bulge in the 2 m contours (Figure 5) is observed offshore of the rip current. The localized 3 m offshore delta is observed offshore of the rip current. The delta extends ~1.25 surf zone widths from the shoreline at about the same distance offshore where the mean currents decayed to zero. A counter flow circulation is believed to have developed near the shoreline, since PUV3 orientation is shoreward for yearday 306 (Fig. 5b) and alongshore for yearday 309 (Fig. 5d). This is similar to laboratory observations by Haller et al. (2002), but until now has not been observed in the field.

Rip currents systems can be classified based on their Froude number (MacMahan et al., 2006), which is similar to quantifying the importance of wave-current interactions (Haller and Okzan-Haller, 2002). U=Cg within the shallow water limit of linear theory is $U/\sqrt{gh}$, referred to as the Froude number, where h is the local water depth and g is the gravitational acceleration. The Froude number ranges 0 to 1 and is used to evaluate the importance of wave-current interaction for a rip current system. The mean Froude number of PUV11 was 0.08 for seaward-directed flows indicating weak wave-current interaction. We classify this rip current system as low energy. A maximum Froude number of 0.25 was estimated for yearday 309 during low-tide, when the rip current velocity reached 0.5 m/s, increasing the importance of wave-current interaction. The wave-current interactions are evaluated in Section 5.

4. Alongshore non-uniformity

4.1. Bathymetric non-uniformity

Non-uniformities of bathymetry can induce alongshore variations in radiation stresses and pressure gradients to drive circulation (Bowen, 1969; Dalrymple, 1978). A measure of bathymetric non-uniformity (Feddersen and Guza, 2003) is the along-shore depth standard deviation, $\sigma_h(x)$, defined

$$\sigma_h(x) = \sqrt{\frac{1}{L_y}\int_0^{Ly}\left(h(x,y)-\overline{h(x)}\right)^2 dy}, \quad (1)$$

where $h(x,y)$ is the bathymetry between $-50 \le x \le 200$ and $2200 \le y \le 2800$, and $\overline{h(x)}$ is the alongshore mean cross-shore profile. Owing to the fact that the contour lines are not parallel to the y-axis, contour lines are rotated (~2°), so that 0 m contour line is parallel to the local y-axis. Note x', $y'=(0,0)$ in the rotated coordinate frame corresponds to $x,y=50$, 2500 in Fig. 1. $\overline{h(x')}$ and $\sigma_h(x')$ are similar for the 6 surveys, with $\sigma_h(x')$ reaching maxima values of 0.24–0.37 m in 2.6 m water depth (Fig. 6). The $\sigma_h(x')$ values are greatest in the region of breaking waves, where the width of

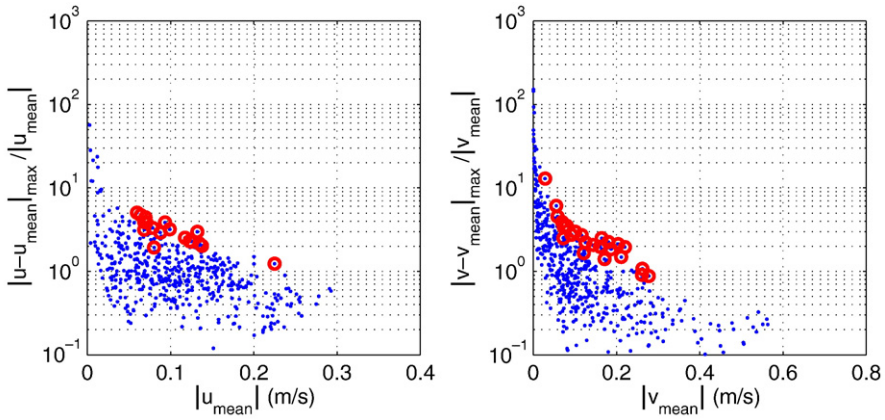

Fig. 7. Alongshore kinematic uniformity for the cross- (left) and alongshore (right) velocity components for yeardays 302-322. Circles represent hourly events that are non-uniform.

the non-uniformity region is associated with the horizontal excursion (~100 *m*) of the break point over a 2 m tide on a 1:50 beach slope (Thornton and Kim, 1993). The non-uniformity of this beach is predominantly associated with the offshore rip morphology (area of accretion) and not with the surfzone rip channels.

4.2. Alongshore kinematic velocity non-uniformity

Non-uniformities of cross- and alongshore velocity components of the along-shore array are determined by maximum hourly mean deviation ($\delta\bar{u}_{max}=\max(\bar{U}-\bar{u})$, $\delta\bar{v}_{max}=\max(\bar{V}-\bar{v})$) of the mean of the mean alongshore array velocities, $\overline{U}=\frac{1}{N}\sum_1^N\overline{u}$, where $\bar{u},\bar{v}$ are the hourly mean velocities at each instrument location and N is the number of observational locations (N=6). $\bar{u}_{max}$, $\bar{v}_{max}$ are compared with the total hourly alongshore surfzone variability $\left(\overline{\sigma}=\sqrt{1/N\sum_1^N(\sigma_u^2+\sigma_v^2)}\right.$, whereas Feddersen and Guza (2003) evaluated maximum alongshore mean deviations compared to current meter noise (σ). Assuming the velocities are Gaussian distributed, there is a 90% probability that

$$|\delta\overline{u}|_{max}/|\overline{U}|\geq 1.476\sqrt{1/N}\overline{\sigma}/|\overline{U}| \quad (2)$$

$$|\delta\overline{v}|_{max}/|\overline{V}|\geq 1.476\sqrt{1/N}\overline{\sigma}/|\overline{V}| \quad (3)$$

where is N is the number of current meters, which is a slightly modified hypothesis test on mean (Bendat and Peirsol, 2000). If greater than 10% of $|\bar{u}|_{max}/|U|$ ($|\bar{v}|_{max}/|V|$) exceeds the alongshore variability of the system, the hypothesis that $\bar{u}$,($\bar{v}$) is alongshore uniform is rejected. The cross- and alongshore velocities at NCEX are predominantly alongshore uniform (circles in Figs. 4, 7 indicate non-uniformities), because Eq. (2), 3 is rejected only 4–5% of the time for five degrees of freedom for six observations. Non-uniformity primarily occurred between yeardays 306–311, when rip currents were active around low-tide (Fig. 4). The pattern of increasing rip current velocities during lower tidal elevations is consistent with previous observations of rip currents (Brander, 1999, MacMahan et al., 2005, amongst others). The bathymetric non-uniformity was persistent throughout bathymetric surveys, while kinematic non-uniformity varied as a function of wave and tidal conditions, and the alongshore location of the bathymetric non-uniformity relative to the instrument locations.

5. Alongshore variability

5.1. Alongshore variability of waves and velocity fields

The alongshore variations of the cross-shore velocity and wave characteristics at the alongshore array (located at ~−1 m depth contour) were calculated for the mean, sea-swell, infragravity, and very low frequency (VLF) frequency bands for two rip current (kinematically non-uniform) days for high and low tide conditions (Fig. 8).

5.2. Infragravity rip current pulsations (0.004<*f*<0.04 Hz)

MacMahan et al. (2004a) determined that low frequency (infragravity) rip current pulsations were forced by standing infragravity waves for a high-energy, steep-sloping, reflective beach characterized by transverse bars with incised rip channels. This hypothesis is evaluated for this low-energy mild-sloping dissipative beach. Coherence and phase spectra are estimated from the average of four demeaned, quadratically detrended (to remove tides) 15 min segments with 50% overlap between p and u at PUV11 (in the rip channel) and PUV12 (on the shoal) for yearday 309 (Fig. 9). The coherence (γ^2) varies between 0 and 0.7 within the infragravity band (0.004<f<0.04Hz), whereas the coherency is 1 for the sea-swell band (>0.04 Hz). The phase (θ) varies between −90° and +90° within the infragravity band indicative of standing waves (Suhayda, 1974), and is zero for the sea-swell band indicative of progressive waves, consistent with previous field observations at Torrey Pines on a mild sloping beach (Huntley et al., 1981; Guza and Thornton, 1985) and during RIPEX (RIP Current EXperiment in Monterey Bay, CA) for a steep beach (MacMahan et al., 2004a). The infragravity velocity is smaller within the rip channels at low tide owing to the relatively greater depths of the rip channels compared with at high tide (Fig. 8b) (see MacMahan et al., 2004a). The long wave relationship ignoring bottom slope effects is defined as

$$U_{rms,ig}=\eta_{rms,ig}\sqrt{\frac{g}{h}} \quad (4)$$

where $U_{rms,ig}$ is $\sqrt{u_{rms,ig}^2+v_{rms,ig}^2}$, g is the gravitational acceleration, and h is the local water depth (Dean and Dalrymple, 1984). Infragravity velocities are modeled using Eq. (4) for low-tide. The results are similar to the alongshore observations, decreasing in the vicinity of the rip channel, but are slightly lower in magnitude (Fig. 8b). Thus, standing infragravity motions contribute to the forcing of rip current pulsations. The rms infragravity velocity is on the order of 15 cm/s, which is approximately 40% of the measured mean rip current flow velocity.

5.3. Very low frequency motions (<0.004 Hz)

Energy at frequencies <0.004 Hz and outside the gravity restoring region delineated by the mode zero edge wave curve, is due to very low frequency (VLF) motions (see MacMahan et al., 2004a,b, 2006; Reniers et al., 2007). The VLFs have been associated with the presence of rip currents (Smith and Largier, 1995; Haller and Dalrymple, 2001; Brander

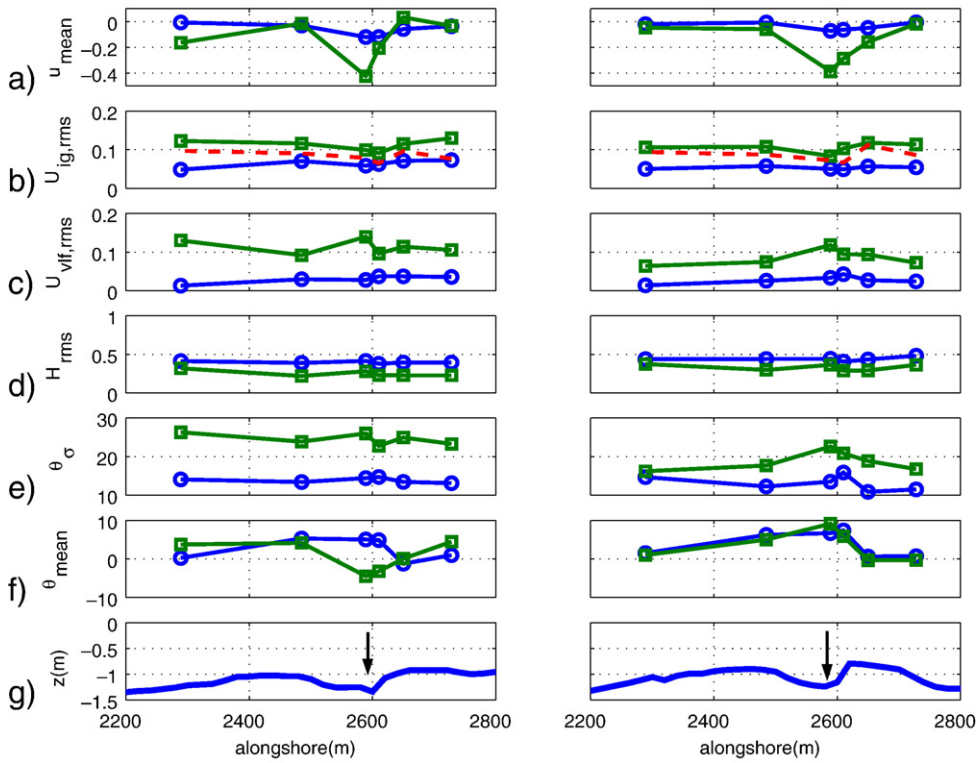

Fig. 8. Alongshore variations of hourly u_{mean} (a), $U_{\text{ig,rms}}$ (b), $U_{\text{vlf,rms}}$ (c), H_{rms} (d), σ_{mean} (e), θ_{mean} (f), and alongshore bathymetric (g) measurements within the alongshore array for yeardays 306 (left panels) and 309 (right panels). Circles represent high tide and squares represent low tide. The dashed line represents modelled estimates of $U_{\text{ig,rms}}$ at low tide for $U_{\text{ig,rms}}$. Arrows indicate the rip channel.

and Short,2001; MacMahan et al., 2004b). The source of rip current VLF motions has been attributed to two mechanisms. The first mechanism was identified as an instability for the case of monochromatic waves and high rip current jet shear conditions in the laboratory (Haller and Dalrymple, 2001) and in a model (Yu and Slinn, 2003). For rip current shear instabilities, the VLF energy is predicted to be significantly larger

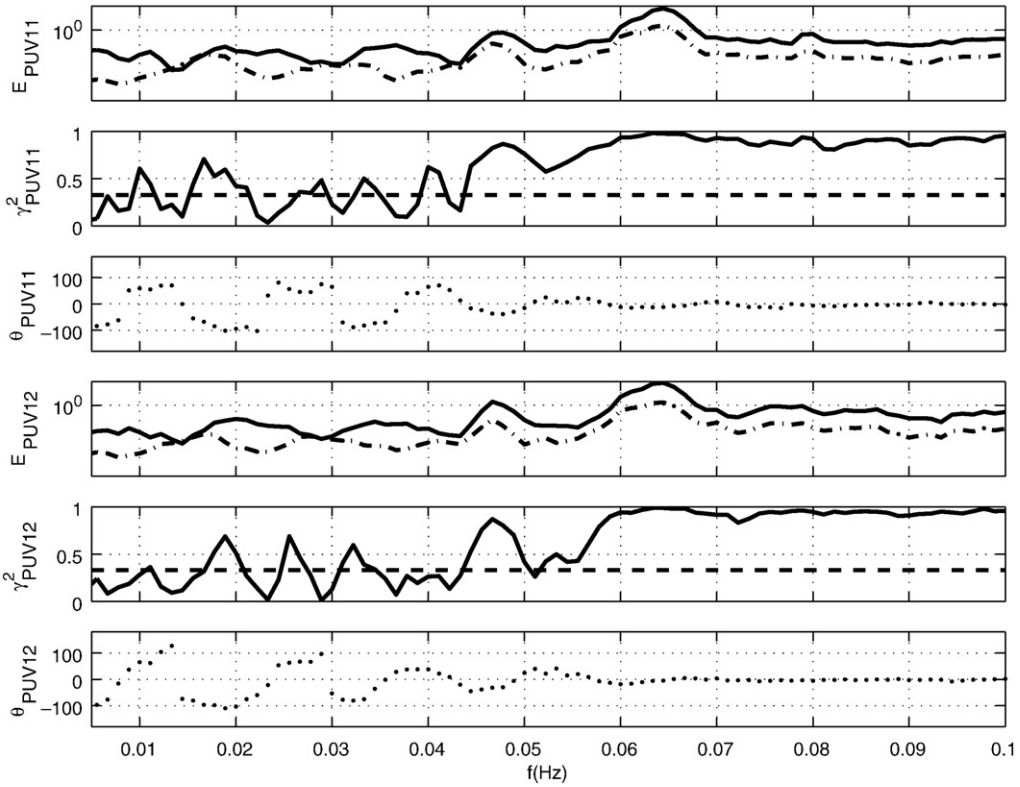

Fig. 9. Energy, coherency (γ^2), and phase (θ) spectra for pressure (solid line) and cross-shore velocity (dashed line) estimates for PUV11 (top three sub-panels) and PUV12 (bottom three sub-panels) for yearday 309.27. Dash lined for γ^2 spectra represent confidence limit.

outside the surf zone than inside the surf zone (Yu and Slinn, 2003; Reniers et al., 2007), whereas the laboratory measurements of Haller and Dalrymple (2001) found maximum VLF variance at the rip throat.

The second mechanism suggests that VLFs are surf zone eddies generated by wave groups that can potentially be coupled to the rip current morphology (MacMahan et al., 2004b; Reniers et al., 2004, 2007). Reniers et al. (2007) determined through modeling that rip current related VLFs can be discriminated between rip current shear instabilities and surf zone eddies by the cross-shore distribution of the VLF velocities. For surf zone eddies forced by directionally spread random waves, the VLF velocities have a maximum within the surf zone and decrease shoreward and seaward (Reniers et al., 2007), whereas rip current shear instabilities have a maximum outside the surf zone (Yu and Slinn, 2003).

The alongshore spatial distributions of VLF velocities (Fig. 8c) indicate that these motions are maxima within the vicinity of the rip currents at the alongshore distance 2600 m (Fig. 8c). Shear instabilities of the rip current jet appear to contribute to a local maximum of VLF velocity within the rip current. For RIPEX, the VLFs were alongshore uniform, while NCEX has alongshore variability. The rip channels for RIPEX were relatively close together ($\lambda = 125$ m), suggesting rip currents were dependent upon each other, whereas for NCEX the rip currents are much further apart ($\lambda > 300$ m) and appear independent of each other (Fig. 4).

The generation of background VLF energy away from the rip current is hypothesized to develop by mechanism two (Reniers et al., 2004; MacMahan et al., submitted for publication). VLF energy increases with increasing wave height, while increasing deep-water directional spreading modifies the alongshore spatial scale (Reniers et al., 2004; MacMahan et al., submitted for publication). VLF energy for NCEX is related to the incoming sea-swell energy and modulated by the tide, similar to results by MacMahan et al. (2004b) at RIPEX (not shown). The rms VLF velocity was on the order 10 cm/s, which is approximately 25% of the measured mean rip current flow.

5.4. Short-waves (H_{rms})

The one-hour mean cross-shore currents show well-defined rip currents flowing offshore at low tide and disappearing at high tide. The largest velocity variations within the surf zone are due to tides. In general, the rip current velocity is maximum at low tide (Aagaard et al., 1997; Brander, 1999; Brander and Short, 2000, 2001; MacMahan et al., 2005). It is hypothesized that the increase in rip current velocity is due: 1) to the decrease in tidal elevation modifying wave breaking, which affects the corresponding pressure and radiation stress gradients, and 2) to the constriction of the rip current channel owing to continuity.

The H_{rms} statistically varies alongshore at the 95% level of significance for either low or high tide (Fig. 8d), suggesting that the alongshore pressure and radiation stress gradients are important, even though the alongshore variability is small.

5.5. Wave direction and directional spreading

The mean wave direction (θ_{mean}) and directional spreading ($\sigma\theta$) are computed utilizing the low-order Fourier moments of directional-frequency wave spectra (Kuik et al., 1990; Herbers et al., 1999). The measured directional spreading increases at low tide and within the vicinity of the rip current maximum (Fig. 8e). Herbers et al. (1999) found that directional spreading increases shoreward, in particular, within the surf zone on an alongshore uniform beach. Thus, the directional spreading increases at low tide within the saturated surf zone.

The increase in directional spreading within the vicinity of the rip channel is hypothesized to be a result of increased wave refraction by the rip current, bathymetry, and rip current pulsations. When the mean rip current maximum migrates in the alongshore, so does the maximum directional spreading (Fig. 8e). Though significantly correlated at 95% confidence interval, the correlation between (σ_θ) and U_{mean} for the alongshore array for yeardays 305–320 is low, $r^2 = 0.16$ (Fig. 10). Henderson et al. (2006) suggested that the increase in directional spreading within the surf zone, as observed by Herbers et al. (1999), is due to wave refraction owing to the offshore current fluctuations of the shear instabilities. Since the shear instabilities were alongshore uniform, the directional spreading was relatively alongshore uniform. Here, the rip current VLF pulsations provide current fluctuations that increase the variability of the local wave directions, which increases the directional spreading. The alongshore directional spreading varies alongshore and is correlated better with $U_{\mathrm{rms},vlf}$, ($r^2 = 0.48$), supporting the notion that the presence of the rip current increases the $U_{\mathrm{rms},vlf}$, which increases (σ_θ) (Fig. 8e, 10).

The wave direction varies within the rip channel, with a reversal in mean wave direction about shore-normal at low tide on yearday 306 (Fig. 8f). This suggests wave convergence into the rip current as described by Dalrymple and Loranzo (1978) and Yu and Slinn (2003), but it was shown that the wave–current interaction had minimal affects on the wave height at 1 m contour. The existence of the small rip current delta at 3 m is hypothesized to provide a positive feedback on the rip current circulation during low tide and modify the mean wave direction around the vicinity of the rip current observations.

7. Summary

The rip current location was coupled to a surprisingly small alongshore perturbation on the bathymetry comprising the rip channel. The rip channel spacing was ~300 m with a ~140 m channel width with a depth variation across the rip channel of only ~0.25 m.

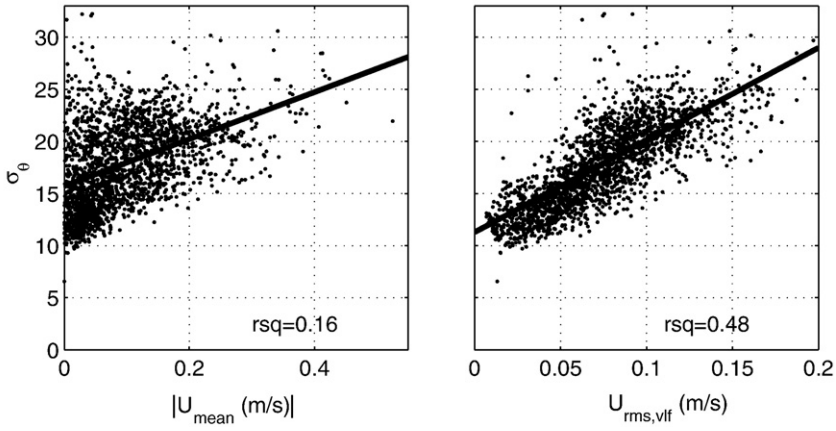

Fig. 10. Directional spreading, (σ_θ), versus U_{mean} (left) and $U_{\mathrm{rms},vlf}$ (right) for the alongshore array for yeardays 302–322.

The rip current and corresponding morphology migrated alongshore at ~12 m/day. A localized offshore delta was identified as a seaward bulge in the 2 m contours and was observed offshore of the rip current. The delta extended ~1.25 surf zone widths from the shoreline to about the same distance offshore where the mean currents decayed to zero.

The subtle bathymetric variation and low energy rip current modified the alongshore variability of wave heights, infragravity motions, VLF motions, directional spreading, and wave direction. Infragravity rip current pulsations had minima in the alongshore in the vicinity of the rip current owing to the deeper channels, consistent with shallow water long wave theory. VLFs had maxima in the vicinity of the rip current. The rip current VLF fluctuations increased directional wave spreading within the rip channel. The rip current delta is hypothesized to modify the local wave direction. These observations demonstrate that small bathymetric non-uniformities can have significant effects on surf zone hydrodynamics highlighting the requirement of alongshore field observations and detailed bathymetric surveys.

Acknowledgements

We thank many folks who assisted in obtaining a great data set: Ron Cowen, Mark Orzech, Jim Stockel, John Woods, Keith Wyckoff, and Rob Wyland. We thank Tom Lippmann and his OSU group and Scripps for performing bathy-metric surveys. Cindy Paden, Rob Holman, and Kristen Splinter provided ex-tended rectified Argus images. JM was funded by ONR under contract number N00014-05-1-0154 and N00014-05-1-0352 and the Naval Postgraduate School. EBT and TPS were funded by ONR under contracts N0001405WR20150 and N0001405WR20385. AJHMR was funded by ONR under contract N000140310829 and the Dutch National Science Foundation (NWO) under contract DCB.5856. GS was a National Research Council Fellow during a sabatical funded in part by the ONR under contract N0001405WR20150.

References

Aagaard, T., Greenwood, B., Nielsen, J., 1997. Mean currents and sediment transport in a rip channel. Mar. Geol. 140, 24–45.
Bendat, J.S., Piersol, A.G., 2000. Random data analysis and measurement procedures, 3 rd edition. John Wiley Series.
Bowen, A.J., 1969. Rip currents, 1, Theoretical investigations. J. Geophys. Res. 74, 5467–5478.
Brander, R.W., 1999. Field observations on the morphodynamic evolution of low wave energy rip current system. Mar. Geol. 157, 199–217.
Brander, R.W., Short, A.D., 2000. Morphodynamics of a large-scale rip current system at Muriwai Beach, New Zealand. Mar. Geol. 165, 27–39.
Brander, R.W., Short, A.D., 2001. Flow kinematics of low-energy rip current systems. J. Coastal Res. 17 (2), 468–481.
Callaghan, D.P., Baldock, T.E., Nielsen, P., Hanes, D.M., Hass, K., MacMahan, J.H., 2004. Pulsing and circulation in a rip current system. Proceedings of the 29th International Conference on Coastal Engineering. Am. Soc. of Civ. Eng., Portugal pp. 1493–1505.
Dalrymple, R.A., 1978. Rip currents and their genesis. Summaries, 16th International Conference on Coastal Engineering, Conference Paper No 140.
Dalrymple, R.A., Lozano, C.J., 1978. Wave-current interation models for rip currents. J. Geophys. Res. 83 (C12), 6063–6071.
Dean, R.G., Dalrymple, R.A., 1984. Water Wave Mechanics for Engineers and Scientists. Prentice-Hall, New Jersey.
Feddersen, F., Guza, R.T., 2003. Observations of nearshore circulation: alongshore uniformity. J. Geophys. Res. 108 (C1), 3006. doi:10.1029/2001JC001293.
Guza, R.T., Thornton, E.B., 1985. Observations of surf beat. J. of Geophys. Res. 90, 3161–3171.
Haller, M.C., Dalrymple, R.A., 2001. Rip current instabilities. J. Fluid Mech. 433, 161–192.
Haller, M.C., Ozkan-Haller, T., 2002. Wave breaking and rip current circulation. paper presented at international conference on coastal engineering. Am. Soc. of Civil Eng. 705–717 Cardiff.
Haller, M.C., Dalrymple, R.A., Svendsen, I.A., 2002. Experimental study of nearshore dynamics on a barred beach with rip channels. J. Geophs. Res. 107 (14), 1–21.
Henderson, S.M., Guza, R.T., Elgar, S., Herbers, T.H.C., 2006. Refraction of surface gravity waves by shear waves. J. Physical Oceanography 36 (4), 629635.
Herbers, T.H.C., Elgar, S., Guza, R.T., 1999. Directional spreading of waves in the nearshore. J. Geophys. Res. 104 (C4), 7683–7693.
Huntley, D.A., Guza, R.T., Thornton, E.B., 1981. Field observations of surf beat, Part I: Progressive edge waves. J. of Geophys. Res. 86, 6451–6466.
Kuik, A.J., van Vledder, G.P., Holthuijzen, L.H., 1990. A method for the routine analysis of pitch-and-roll bouy data. J. Phys. Oceanogr. 18, 1020–1034.
Long, J.W., Ozkan-Haller, H.T., 2005. Offshore controls on nearshore rip currents. J. Geophys. Res. 110 (C12007). doi:10.1029/2005JC003018.
MacMahan, J., Reniers, A.J.H.M., Thornton, E.B., Stanton, T., 2004a. Infragravity rip current pulsations. J. of Geophys. Res. 109 (C01033). doi:10.1029/2003JC002068.
MacMahan, J.H., Reniers, A.J.H.M., Thornton, E.B., Stanton, T.P., 2004b. Surf zone eddies coupled with rip current morphology. J. Geophys Res. 109 (C07004). doi:10.1029/2003JC002083.
MacMahan, J., Thornton, E.B., Reniers, A.J.H.M., 2006. Rip current review. J. Coast. Eng. 53 (2–3), 191–208. doi:10.1016/j.coastaleng.2005.10.009.
MacMahan, E.B., Thornton, T., Stanton, Reniers, A.J.H.M., 2005. RIPEX-rip currents on a shore-connected shoal beach. Mar. Geol.
MacMahan, J., J. Brown, A.J.H.M. Reniers, J. Brown, E.B. Thornton, T.P. Stanton, Gallagher, E., submitted for publication. Lagrangian observations on a rip-channeled beach. Geophys. Res. Lett.
Reniers, A.J.H.M., Roelvink, J.A., Thornton, E.B., 2004. Morphodynamic modeling of an embayed beach under wave group forcing. J. of Geophys. Res. 109 (C01030). doi:10.1029/2002JC001586.
Reniers, A., MacMahan, J., Thornton, E.B., Stanton, T.P., 2007. Modeling of very low frequency motions during RIPEX. J. Geophys. Res. doi:10.1029/2005JC003122.
Shepard, F.P., Inman, D.L., 1950. Nearshore water circulation related to bottom topography and refraction. Trans. Am. Geophys, 31. Union, pp. 196–212.
Shepard, F.P., Emery, K.O., La Fond, E.C., 1941. Rip currents: a process of geological importance. J. Geol. 49, 337–369.
Smith, J.A., Largier, J.L., 1995. Observations of nearshore circulation: rip currents. J. Geophys. Res. 100, 10967–10975.
Sonu, C.J., 1972. Field observations of nearshore circulation and meandering currents. J. Geophys. Res. 77, 3232–3247.
Suhayda, J.N., 1974. Standing waves on beaches. J. of Geophys. Res. 79, 3065–3071.
Thornton, E.B., Kim, C.S., 1993. Longshore current and wave height. Modulation at tidal frequency inside the surf zone. J. Geophys. Res. 98 (C9) 16,509 16,519.
Yu, J., Slinn, D.N., 2003. Effects of wave-current interaction on rip currents. J. Geophys. Res. 108, 3088. doi:10.1029/2001JC001105.